Axisymmetric thermo-mechanical analysis of laser-driven non-contact transfer printing

Rui Li, Yuhang Li, Chaofeng Lü, Jizhou Song, Reza Saeidpourazar, Bo Fang, Yang Zhong, Placid M. Ferreira, John A. Rogers, et al.

International Journal of Fracture

ISSN 0376-9429
Volume 176
Number 2

Int J Fract (2012) 176:189-194
DOI 10.1007/s10704-012-9744-9

Springer

Int J Fract (2012) 176:189–194
DOI 10.1007/s10704-012-9744-9

ORIGINL PAPER

Axisymmetric thermo-mechanical analysis of laser-driven non-contact transfer printing

Rui Li · Yuhang Li · Chaofeng Lü · Jizhou Song · Reza Saeidpourazar · Bo Fang · Yang Zhong · Placid M. Ferreira · John A. Rogers · Yonggang Huang

Received: 1 May 2012 / Accepted: 14 June 2012 / Published online: 11 July 2012

Abstract An axisymmetric thermo-mechanical model is developed for laser-driven non-contact transfer printing, which involves laser-induced impulsive heating to initiate separation at the interface between a soft, elastomeric stamp and hard micro/nanomaterials (i.e., inks) on its surface, due to a large mismatch in coefficients of thermal expansion. The result is the active ejection of the inks from the stamp, to a spatially separated receiving substrate, thereby representing the printing step. The model gives analytically the temperature field, and also a scaling law for the energy release rate for delamination at the interface between the stamp and an ink in the form of a rigid plate. The normalized critical laser pulse time for interfacial delamination depends only on the normalized absorbed laser power and width of the ink structure, and has been verified by experiments.

Keywords Laser-driven non-contact transfer printing · Thermo-mechanical analysis · Axisymmetric model · Stamp and ink

1 Introduction

Laser-driven non-contact transfer printing is a new technique for materials assembly and micro-/nanofabrication. Micro/nanoscale materials, such as wires, membranes, platelets, etc, are retrieved (i.e., picked up) from a growth (donor) substrate via an elastomeric

Rui Li and Yuhang Li contributed equally to this work.

R. Li · Y. Zhong
Department of Engineering Mechanics, State Key Laboratory of Structural Analysis for Industrial Equipment, Dalian University of Technology, Dalian 116024, China

R. Li · Y. Li · C. Lü · Y. Huang (✉)
Department of Civil and Environmental Engineering, Northwestern University, Evanston, IL 60208, USA
e-mail: y-huang@northwestern.edu

R. Li · Y. Li · C. Lü · Y. Huang
Department of Mechanical Engineering, Northwestern University, Evanston, IL 60208, USA

Y. Li · B. Fang
School of Astronautics, Harbin Institute of Technology, Harbin 150001, China

C. Lü
Department of Civil Engineering, Soft Matter Research Center, Zhejiang University, Hangzhou 310058, China

J. Song
Department of Mechanical and Aerospace Engineering, University of Miami, Coral Gables, FL 33146, USA

R. Saeidpourazar · J. A. Rogers
Department of Materials Science and Engineering, University of Illinois, Urbana, IL 61801, USA

R. Saeidpourazar · P. M. Ferreira · J. A. Rogers
Department of Mechanical Science and Engineering, University of Illinois, Urbana, IL 61801, USA

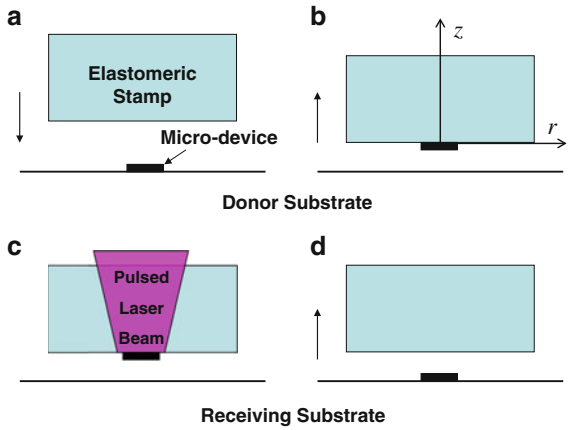

Fig. 1 Schematic illustration of the laser transfer printing process: **a** the stamp is aligned with a donor substrate to retrieve the ink, illustrated here as a micro-device; **b** the micro-device is lifted onto the surface of the stamp; **c** the stamp is aligned to a receiving substrate and a laser pulse is used to deliver heat to the interface between the micro-device and the stamp; and **d** the micro-device is transferred to the receiving substrate and the stamp is withdrawn for the next printing cycle

stamp, and then printed onto a different (receiver) substrate without direct contact (Meitl et al. 2006). A laser pulse initiates separation at the adhesive surface due to large thermal mismatch between the stamp and ink. As illustrated in Fig. 1, the process starts with retrieval of inks from a donor substrate (Fig. 1a, b) with an elastomeric (e.g., PDMS). The 'inked' stamp is then brought close (a few micrometers) to the receiving substrate (Fig. 1c). A pulsed laser beam, focusing on the stamp/ink interface, causes the active ejection of the inks from the stamp such that they land on the receiving substrate (Fig. 1d).

Laser-driven non-contact transfer printing can be valuable for advanced engineering development of systems such as stretchable/flexible semiconductor devices for structural health monitoring (Nathan et al. 2000), image sensors (Lumelsky et al. 2001; Mannsfeld et al. 2010; Someya et al. 2005; Someya and Sekitani 2009), flexible display (Crawford 2005; Forrest 2004; Gelinck et al. 2004), deformable circuits (Kim et al. 2008; Sekitani et al. 2010) flexible inorganic solar cells (Yoon et al. 2008) and LEDs (Sekitani et al. 2009). It can integrate high-performance inorganic semiconductor materials, in ultrathin geometries, with substrates of interest, such as sheets of plastic or slabs or rubber. The resulting components can be of particular value in biomedical devices such as smart surgical gloves (Someya et al. 2004), in biomimetic, curvilinear electronics (Ko et al. 2008), bio-dissolvable electronics (Kim et al. 2010a), monitors for cardiac electrophysiology (Viventi et al. 2010) and ablation therapy (Kim et al. 2011a), foldable electrode arrays for mapping brain activity (Viventi et al. 2011), waterproof optoelectronics for diagnostics (Kim et al. 2010b), and epidermal electronics for health/wellness evaluation and brain-machine interfaces (Kim et al. 2011b).

A two-dimensional (plane-strain) thermo-mechanical model for laser-driven non-contact transfer printing (Li et al. 2012) has identified that the mismatch between the thermo-mechanical properties of the stamp and ink drives their interfacial delamination. The purpose of this paper is to develop a more realistic, axisymmetric thermo-mechanical model for laser-driven non-contact transfer printing. A scaling law is established to identify a single non-dimensional combination of material and geometry parameters that control laser-driven non-contact transfer printing. The scaling law agrees very well with the experiments, and is useful to optimal design of stamp for transfer printing.

2 Heat conduction

An axisymmetric model of heat conduction is established for the laser-driven non-contact transfer printing illustrated in Fig. 1c. The ink has radius r_{ink} and thickness h_{ink} attached to a large elastomeric stamp, which is modeled as a semi-infinite solid (Saeidpourazar et al. 2012). The absorbed laser power by the ink is denoted by P.

The transient heat conduction equation in the stamp is (Incropera et al. 2007)

$$\frac{\partial^2\theta_{\text{stamp}}}{\partial r^2}+\frac{1}{r}\frac{\partial\theta_{\text{stamp}}}{\partial r}+\frac{\partial^2\theta_{\text{stamp}}}{\partial z^2}-\frac{c_{\text{stamp}}\rho_{\text{stamp}}}{\lambda_{\text{stamp}}}\frac{\partial\theta_{\text{stamp}}}{\partial t}=0 \tag{1}$$

with the initial condition $\theta_{\text{stamp}}\big|_{t=0}=0$, where (r, z) are the cylindrical coordinates (Fig. 1b), t is time, θ_{stamp} is the temperature increase from the ambient temperature, and c_{stamp}, ρ_{stamp} and λ_{stamp} are the specific heat, mass density and thermal conductivity of the stamp, respectively. The natural convection on the stamp surface is negligible because of the short duration of pulsed laser beam. This gives the boundary condition

$$-\lambda_{\text{stamp}}\left.\frac{\partial\theta_{\text{stamp}}}{\partial z}\right|_{z=0}=\begin{cases}q\,(t) & \text{for } 0\le r\le r_{\text{ink}}\\ 0 & \text{for } r>r_{\text{ink}}\end{cases}, \quad (2)$$

where $q\,(t)$ is the heat flux into the stamp. It is obtained approximately in the "Appendix" as

$$q\,(t)=\frac{P}{\pi r_{\text{ink}}^2}\left[1-\exp\left(\frac{t}{t_0}\right)\text{erfc}\left(\sqrt{\frac{t}{t_0}}\right)\right], \quad (3)$$

where erfc is the complementary error function (Fettis et al. 1973),

$$t_0=\frac{c_{\text{ink}}^2\rho_{\text{ink}}^2h_{\text{ink}}^2}{c_{\text{stamp}}\rho_{\text{stamp}}\lambda_{\text{stamp}}} \quad (4)$$

represents the characteristic time in laser-driven non-contact transfer printing, and c_{ink} and ρ_{ink} are the specific heat and mass density of the ink, respectively.

The Hankel transform and Fourier cosine transform (with respect to r and z, respectively) of Eq. (1) gives an ordinary differential equation with respect to t. Its solution is obtained analytically. The inverse transforms give the temperature increase in the stamp as

$$\theta_{\text{stamp}}(r,z,t)=\frac{c_{\text{ink}}\rho_{\text{ink}}h_{\text{ink}}}{c_{\text{stamp}}\rho_{\text{stamp}}\lambda_{\text{stamp}}}\frac{P}{\sqrt{\pi^3}r_{\text{ink}}^2}\times\left\{\int_0^{t'}\frac{1-\exp\left(t'-\tau\right)\text{erfc}\sqrt{t'-\tau}}{\sqrt{\tau}}\exp\left[\frac{-z'^2\left(r'_{\text{ink}}\right)^2}{4\tau}\right]\text{d}\tau\right.$$
$$\left.\times\int_0^{\infty}J_0\left(r'\eta\right)J_1\left(\eta\right)\exp\left[\frac{-\tau\eta^2}{\left(r'_{\text{ink}}\right)^2}\right]\text{d}\eta\right\}, \quad (5)$$

where $r'=r/r_{\text{ink}}$ and $z'=z/r_{\text{ink}}$ are the normalized coordinates, $t'=t/t_0$ is the normalized time, and

$$r'_{\text{ink}}=\frac{c_{\text{stamp}}\rho_{\text{stamp}}r_{\text{ink}}}{c_{\text{ink}}\rho_{\text{ink}}h_{\text{ink}}}. \quad (6)$$

is the normalized radius of the ink.

Equation (5) suggests that the temperature increase, normalized by $c_{\text{ink}}\rho_{\text{ink}}h_{\text{ink}}P/(c_{\text{stamp}}\rho_{\text{stamp}}\lambda_{\text{stamp}}r_{\text{ink}}^2)$, depends on the normalized position (r' and z') and time (t'), and a single combination of stamp and ink properties $r'_{\text{ink}}=c_{\text{stamp}}\rho_{\text{stamp}}r_{\text{ink}}/(c_{\text{ink}}\rho_{\text{ink}}h_{\text{ink}})$. Figure 2 shows the normalized distribution of temperature increase in the radial direction for $z'=z/r_{\text{ink}}=0$, 0.1 and 0.2, normalized time $t'=8.90$ and $r'_{\text{ink}}=16.4$, which corresponds to $c_{\text{ink}}=708\ \text{J kg}^{-1}\text{K}^{-1}$, $\rho_{\text{ink}}=2.30\times10^3\ \text{kg m}^{-3}$ for silicon (Campbell 2001), $c_{\text{stamp}}=1.46\ \text{kJ kg}^{-1}\text{K}^{-1}$, $\rho_{\text{stamp}}=970\ \text{kg m}^{-3}$ for PDMS (Mark 1999), and $r_{\text{ink}}=56.4\,\mu\text{m}$ and $h_{\text{ink}}=3\,\mu\text{m}$ in the experiment (Saeidpourazar et al. 2012).

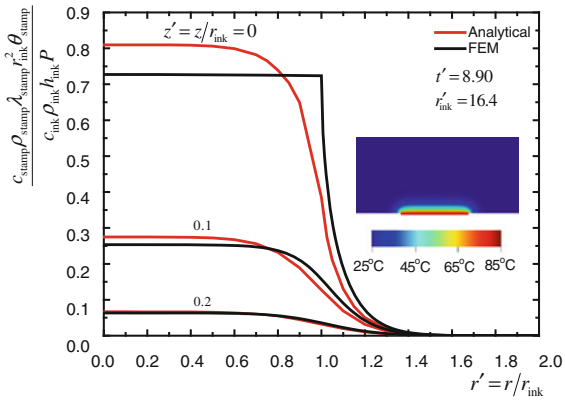

Fig. 2 Distribution of normalized temperature increase in the stamp

Finite element method (FEM) is used to obtain the temperature distributions in the stamp and ink. The ink is modeled as a heat source with the total heat flux $P/(\pi r_{\text{ink}}^2)$. As shown in Fig. 2, the numerical results agree reasonably with the analytical expression in Eq. (5). A contour plot of the temperature field in the cross section cut along the symmetry axis z is included as an inset in Fig. 2.

The temperature increase in the ink is nearly uniform because its thermal conductivity λ_{ink} (e.g., 160 $\text{W m}^{-1}\text{K}^{-1}$ for silicon) (Campbell 2001) is three orders of magnitude larger than λ_{stamp} (e.g., 0.15 $\text{W m}^{-1}\text{K}^{-1}$ for PDMS) (Mark 1999). It is obtained analytically as

$$\theta_{\text{ink}}\,(t)=\frac{c_{\text{ink}}\rho_{\text{ink}}h_{\text{ink}}}{c_{\text{stamp}}\rho_{\text{stamp}}\lambda_{\text{stamp}}}\times\frac{2P}{\sqrt{\pi^3}r_{\text{ink}}^2}\int_0^{t'}\frac{1-\exp\left(t'-\tau\right)\text{erfc}\sqrt{t'-\tau}}{\sqrt{\tau}}\text{d}\tau$$
$$\times\int_0^{\infty}\frac{J_1^2\,(\eta)}{\eta}\exp\left[\frac{-\tau\eta^2}{\left(r'_{\text{ink}}\right)^2}\right]\text{d}\eta. \quad (7)$$

The normalized temperature increase in the ink, $c_{\text{stamp}}\rho_{\text{stamp}}\lambda_{\text{stamp}}r_{\text{ink}}^2\theta_{\text{ink}}/(c_{\text{ink}}\rho_{\text{ink}}h_{\text{ink}}P)$, versus the normalized time t' depends only on the same single combination of stamp and ink properties as in Eq. (6). As shown in Fig. 3 for the same properties and parameters as in Fig. 2, Eq. (7) agrees well with the numerical results obtained by FEM.

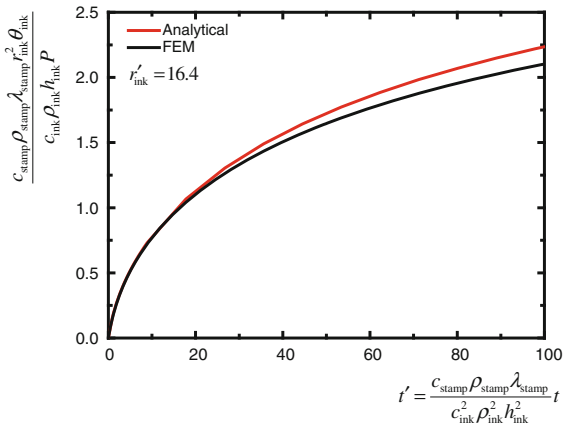

Fig. 3 The normalized temperature increase in the ink

3 Stamp/ink interfacial delamination

The temperature increase in Sect. 2 yields the thermal strain $\alpha_{stamp}\theta_{stamp}$ in the stamp, which drives delamination of the stamp/ink interface, where α_{stamp} is the coefficient of thermal expansion (CTE) of the stamp (e.g., $3.1 \times 10^{-4}\mathrm{K}^{-1}$ for PDMS) (Mark 1999). The CTE of the ink (e.g., $2.6 \times 10^{-6}\mathrm{K}^{-1}$ for silicon) (Okada and Tokumaru 1984) is two orders of magnitude smaller such that the thermal strain in the ink is negligible for stamp/ink interfacial delamination.

For a plane-strain, interfacial crack that lies on $x < 0$, $z = 0$ between two dissimilar materials subjected to a transformation strain over an infinitesimal area $\mathrm{d}x\mathrm{d}z$ around a point (x, z) $(z > 0)$, the complex stress intensity factor is $\sqrt{2/\pi}\mu_{stamp}(\varepsilon_{xx}^{\mathrm{T}} + \varepsilon_{zz}{}^{\mathrm{T}})(x - \mathrm{i}z)^{-3/2}\,\mathrm{d}x\mathrm{d}z$ (Suo 1989), where $\mathrm{i} = \sqrt{-1}$, $\varepsilon_{xx}^{\mathrm{T}}$ and $\varepsilon_{zz}^{\mathrm{T}}$ are the transformation strains, μ_{stamp} is the shear modulus of the stamp, which is five orders of magnitude smaller than that of the ink such that the latter can be considered as rigid (Lu et al. 2007). For an axisymmetric interfacial crack between the stamp and the rigid ink subject to a thermal strain $\alpha_{stamp}\theta_{stamp}$ over a ring with the infinitesimal cross section area $\mathrm{d}r\mathrm{d}z$ around (r, z) $(z > 0)$, the complex stress intensity factor takes the form $\mu_{stamp}\alpha_{stamp}\theta_{stamp}r_{ink}^{-5/2} f\left(\frac{r}{r_{ink}}, \frac{z}{r_{ink}}\right) r\mathrm{d}r\mathrm{d}z$, where f is a non-dimensional function. Its integration over the stamp gives the complex stress intensity factor as

$$K = \mu_{stamp}\alpha_{stamp}r_{ink}^{-5/2} \int_0^{\infty}\int_{r=0}^{\infty} \theta_{stamp}(r, z, t)\, f\left(\frac{r}{r_{ink}}, \frac{z}{r_{ink}}\right) r\mathrm{d}r\mathrm{d}z. \quad (8)$$

Substitution of Eq. (5) into the above expression gives

$$K = \sqrt{\frac{c_{stamp}\rho_{stamp}}{c_{ink}\rho_{ink}h_{ink}}}\frac{\mu_{stamp}\alpha_{stamp}P}{\lambda_{stamp}} \cdot \overline{K}\left(\frac{t}{t_0}, r'_{ink}\right), \quad (9)$$

where $\overline{K}$ is a non-dimensional function of only two variables, the normalized time and ink radius.The interfacial crack tip energy release rate (Suo 1989) $G = |K|^2/(8\mu_{PDMS})$ is given by

$$G = \frac{c_{stamp}\rho_{stamp}\mu_{stamp}\alpha_{stamp}^2P^2}{8c_{ink}\rho_{ink}h_{ink}\lambda_{stamp}^2} \cdot \overline{G}\left(\frac{t}{t_0}, r'_{ink}\right), \quad (10)$$

where $\overline{G}\left(\frac{t}{t_0}, r'_{ink}\right) = \left|\overline{K}\left(\frac{t}{t_0}, r'_{ink}\right)\right|^2$ is also a non-dimensional function of the normalized time and ink radius.

4 Scaling law for the laser pulse time for delamination

The stamp/ink interface delaminates when the interfacial crack tip energy release rate in Eq. (10) reaches the work of adhesion γ of the interface, $G = \gamma$, which, together with Eq. (10), give the critical time $t_{delamination}$ for stamp/ink interfacial delamination,

$$\frac{t_{delamination}}{t_0} = \bar{t}\left(\frac{P}{P_0}, \frac{r_{ink}}{r_0}\right), \quad (11)$$

where $\bar{t}$ is a non-dimensional function, t_0 is given in Eq. (4), and

$$P_0 = \frac{\lambda_{PDMS}}{\alpha_{PDMS}}\sqrt{\frac{\gamma c_{silicon}\rho_{silicon}h_{silicon}}{c_{PDMS}\rho_{PDMS}\mu_{PDMS}}},$$
$$r_0 = \frac{c_{silicon}\rho_{silicon}h_{silicon}}{c_{PDMS}\rho_{PDMS}}. \quad (12)$$

Even though the function $\bar{t}$ is not obtained analytically, Eq. (11) gives the scaling law: the normalized critical time for delamination depends only on the normalized absorbed laser power and ink radius. All properties of the stamp, ink and their interface, and the ink thickness come into play only via the normalizations t_0, P_0 and r_0 in Eqs. (4) and (12).

FEM is used to calculate the interfacial crack tip energy release rate for different absorbed laser powers. The ink has radius $r_{ink} = 56.4\,\mu\mathrm{m}$ and thickness $h_{ink} = 3\,\mu\mathrm{m}$, and is modeled as a heat source with different total heat flux $P/(\pi r_{ink}^2)$. The radius and thickness of the stamp are 564 and 300 μm, respectively, which yield the same result as that for an infinite stamp.

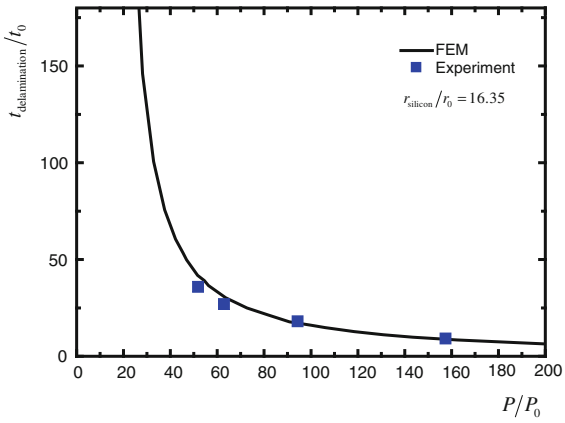

Fig. 4 Scaling law for delamination of the stamp/ink interface

The element CAX8RT for coupled thermal-mechanical analysis in the ABAQUS finite element program (Dassault Systèmes 2009) is used. The crack is located at the end of the stamp/ink interface with the initial crack length 0.1 μm. The boundary condition for the top surface of the stamp is free convection with the coefficient of natural convection 25W m^{-2} K^{-1} (Incropera et al. 2007), while other surfaces are thermal insulated. For a specified work of adhesion, the critical time for different total heat flux is obtained. The critical time is shown versus the laser power in Fig. 4 according to the scaling law in Eq. (11). The laser pulse time of 1, 2, 3 and 4 ms in the experiment correspond to absorbed laser power by the ink ($100 \times 100 \times 3$ μm polished silicon chip) 0.0672, 0.0403, 0.0269 and 0.0222 W, respectively, which give the total heat flux 6.72×10^6, 4.03×10^6, 2.69×10^6 and 2.22×10^6 W m^{-2}. The scaling law agrees very well with the experiments (Saeidpourazar et al. 2012) also shown in Fig. 4.

5 Concluding remarks

Laser-driven non-contact transfer printing involves many thermal and mechanical properties of the stamp, ink, their interface, and the thickness and radius of the ink, and the absorbed laser power P by the ink. A scaling law is established for the critical laser pulse time $t_{\text{delamination}}$ for stamp/ink interfacial delamination; the normalized $t_{\text{delamination}}$ depends only on the normalized power P and radius of the ink r_{ink}. All materials properties and the thickness of the ink h_{ink} come into play only via the normalizations of $t_{\text{delamination}}$, P and r_{ink}.

Acknowledgments The materials presented here are based upon work supported by the Center for Nanoscale Chemical-Electrical-Mechanical System (NanoCEMMS), a Nanoscale Science and Engineering Center sponsored by NSF under Award #0749028 (CMMI). The support from NSF grants ECCS 0824129 and OISE 1043143 is also acknowledged. Y.H. acknowledges the support from NSFC. C.L. acknowledges the support from NSFC by Grant No. 11172263.

Appendix: Heat flux into the stamp

An approximate heat conduction model $\frac{\partial^2 \theta_{\text{stamp}}}{\partial z^2} - \frac{c_{\text{stamp}}\rho_{\text{stamp}}}{\lambda_{\text{stamp}}} \frac{\partial \theta_{\text{stamp}}}{\partial t} = 0$ is adopted to estimate the heat flux into the stamp $q(t)$. The Fourier cosine transform $\tilde{\theta}_{\text{stamp}} = \int_0^\infty \theta_{\text{stamp}}(z) \cos(\beta z)\, \mathrm{d}z$, together with the boundary condition in Eq. (2), give

$$\frac{c_{\text{stamp}}\rho_{\text{stamp}}}{\lambda_{\text{stamp}}} \frac{\partial \tilde{\theta}_{\text{stamp}}}{\partial t} + \beta^2 \tilde{\theta}_{\text{stamp}} = \frac{q(t)}{\lambda_{\text{stamp}}}. \tag{A1}$$

Its solution, satisfying the initial condition $\theta_{\text{stamp}}\big|_{t=0} = 0$, is

$$\tilde{\theta}_{\text{stamp}}(\beta, t) = \frac{1}{c_{\text{stamp}}\rho_{\text{stamp}}} \int_0^t q(\tau) \times \exp\left[-\frac{\lambda_{\text{stamp}}\beta^2}{c_{\text{stamp}}\rho_{\text{stamp}}}(t-\tau)\right] \mathrm{d}\tau. \tag{A2}$$

The inverse Fourier cosine transform then gives

$$\theta_{\text{stamp}}(z=0) = \frac{1}{\sqrt{\pi c_{\text{stamp}}\rho_{\text{stamp}}\lambda_{\text{stamp}}}} \int_0^t \frac{q(\tau)}{\sqrt{t-\tau}} \mathrm{d}\tau. \tag{A3}$$

The temperature increase (from the ambient temperature) in the ink θ_{ink} is nearly uniform because its thermal conductivity λ_{ink} (e.g., 160 W m^{-1} K^{-1} for silicon) (Campbell 2001) is three orders of magnitude larger than λ_{stamp} (0.15 W m^{-1} K^{-1}) (Mark 1999). Its rate of increase is related to the heat flux into the ink $P/(\pi r_{\text{ink}}^2) - q(t)$ by

$$\frac{\mathrm{d}\theta_{\text{ink}}}{\mathrm{d}t} = \frac{P/(\pi r_{\text{ink}}^2) - q(t)}{c_{\text{ink}}\rho_{\text{ink}}h_{\text{ink}}}. \tag{A4}$$

Continuity of temperature across the stamp/ink interface requires

$$\theta_{\text{ink}} = \theta_{\text{stamp}}\big|_{z=0} \quad \text{for} \quad 0 \le r \le r_{\text{ink}}. \tag{A5}$$

Equations (A3)–(A5) give

$$\frac{1}{\sqrt{\pi c_{\text{stamp}}\rho_{\text{stamp}}\lambda_{\text{stamp}}}}\int_0^t \frac{q(\tau)}{\sqrt{t-\tau}}\mathrm{d}\tau = \frac{1}{c_{\text{ink}}\rho_{\text{ink}}h_{\text{ink}}}\left[\frac{P}{\pi r_{\text{ink}}^2}t - \int_0^t q(\tau)\,\mathrm{d}\tau\right], \quad \text{(A6)}$$

which is solved by the Laplace transform to give the solution in Eq. (3).

References

Campbell SA (2001) The science and engineering of microelectronic fabrication. Oxford University Press, New York

Crawford GP (2005) Flexible flat panel display technology. Wiley, New York

Dassault Systèmes (2009) ABAQUS Analysis User's Manual V6.9. Pawtucket

Fettis HE, Caslin JC, Cramer KR (1973) Complex zeros of the error function and of the complementary error function. Math Comput 27:401–407

Forrest SR (2004) The path to ubiquitous and low-cost organic electronic appliances on plastic. Nature 428:911–918

Gelinck GH, Huitema HEA, Van Veenendaal E et al (2004) Flexible active-matrix displays and shift registers based on solution-processed organic transistors. Nat Mater 3:106–110

Incropera FP, DeWitt DP, Bergman TL et al (2007) Fundamentals of heat and mass transfer. Wiley, Hoboken

Kim DH, Ahn JH, Choi WM et al (2008) Stretchable and foldable silicon integrated circuits. Science 320:507–511

Kim DH, Lu NS, Ghaffari R et al (2011) Materials for multifunctional balloon catheters with capabilities in cardiac electrophysiological mapping and ablation therapy. Nat Mater 10:316–323

Kim DH, Lu NS, Ma R et al (2011) Epidermal electronics. Science 333:838–843

Kim DH, Viventi J, Amsden JJ et al (2010) Dissolvable films of silk fibroin for ultrathin conformal bio-integrated electronics. Nat Mater 9:511–517

Kim RH, Kim DH, Xiao JL et al (2010) Waterproof AlInGaP optoelectronics on stretchable substrates with applications in biomedicine and robotics. Nat Mater 9:929–937

Ko HC, Stoykovich MP, Song JZ et al (2008) A hemispherical electronic eye camera based on compressible silicon optoelectronics. Nature 454:748–753

Li R, Li Y, Lü C et al (2012) Thermo-mechanical modeling of laser-driven non-contact transfer printing: two-dimensional analysis. Soft Matter 8:3122–3127

Lu NS, Yoon J, Suo ZG (2007) Delamination of stiff islands patterned on stretchable substrates. Int J Mater Res 98:717–722

Lumelsky VJ, Shur MS, Wagner S (2001) Sensitive skin. Sens J IEEE 1:41–51

Mannsfeld SCB, Tee BCK, Stoltenberg RM et al (2010) Highly sensitive flexible pressure sensors with microstructured rubber dielectric layers. Nat Mater 9:859–864

Mark JE (1999) Polymer data handbook. Oxford University Press, New York

Meitl MA, Zhu ZT, Kumar V et al (2006) Transfer printing by kinetic control of adhesion to an elastomeric stamp. Nat Mater 5:33–38

Nathan A, Park B, Sazonov A et al (2000) Amorphous silicon detector and thin film transistor technology for large-area imaging of X-rays. Microelectron J 31:883–891

Okada Y, Tokumaru Y (1984) Precise determination of lattice-parameter and thermal-expansion coefficient of silicon between 300-K and 1500-K. J Appl Phys 56:314–320

Saeidpourazar R, Li R, Li Y et al (2012) Laser-driven micro-transfer placement of prefabricated microstructures. J Microelectromech Syst. doi:10.1109/JMEMS.2012.2203097

Sekitani T, Nakajima H, Maeda H et al (2009) Stretchable active-matrix organic light-emitting diode display using printable elastic conductors. Nat Mater 8:494–499

Sekitani T, Zschieschang U, Klauk H et al (2010) Flexible organic transistors and circuits with extreme bending stability. Nat Mater 9:1015–1022

Someya T, Kato Y, Sekitani T et al (2005) Conformable, flexible, large-area networks of pressure and thermal sensors with organic transistor active matrixes. Proc Natl Acad Sci USA 102:12321–12325

Someya T, Sekitani T (2009) Printed skin-like large-area flexible sensors and actuators. Proc Eurosens Xxiii Conf 1:9–12

Someya T, Sekitani T, Iba S et al (2004) A large-area, flexible pressure sensor matrix with organic field-effect transistors for artificial skin applications. Proc Natl Acad Sci USA 101:9966–9970

Suo ZG (1989) Singularities interacting with interfaces and cracks. Int J Solids Struct 25:1133–1142

Viventi J, Kim DH, Moss JD et al (2010) A conformal, bio-interfaced class of silicon electronics for mapping cardiac electrophysiology. Sci Transl Med 2:24ra22

Viventi J, Kim DH, Vigeland L et al (2011) Flexible, foldable, actively multiplexed, high-density electrode array for mapping brain activity in vivo. Nat Neurosci 14:1599–1605

Yoon J, Baca AJ, Park SI et al (2008) Ultrathin silicon solar microcells for semitransparent, mechanically flexible and microconcentrator module designs. Nat Mater 7:907–915